ACS Photonics

Article

pubs.acs.org/journal/apchd5

Fabrication of Square-Centimeter Plasmonic Nanoantenna Arrays by Femtosecond Direct Laser Writing Lithography: Effects of Collective Excitations on SEIRA Enhancement

Shahin Bagheri,‡ Ksenia Weber,‡ Timo Gissibl, Thomas Weiss, Frank Neubrech, and Harald Giessen*

4th Physics Institute and Research Center SCoPE, University of Stuttgart, Pfaffenwaldring 57, 70569 Stuttgart, Germany

Supporting Information

ABSTRACT: We demonstrate the use of femtosecond direct laser writing lithography for a fast and homogeneous large-area fabrication of plasmonic nanoantennas on a substrate by creating a patterned polymer as an etch mask on a metal layer. Subsequent argon ion beam etching provides plasmonic nanoantennas with feature sizes below the diffraction limit of the laser light. They exhibit tunable high-quality plasmon resonances in the mid-infrared spectral range, which are ideally suited for surface-enhanced infrared absorption (SEIRA). In the present work, we demonstrate reliable, fast, and low-cost fabrication of a wide variety of antenna arrays and examine particularly the influence of plasmonic coupling between neighboring antennas on the SEIRA enhancement effect. Specifically, we measure the enhanced infrared vibrational bands of a 5 nm thick 4,4′-bis(*N*-carbazolyl)-1,1′-biphenyl layer evaporated on arrays with different longitudinal and transversal spacings between antennas. An optimum SEIRA enhancement per antenna of 4 orders of magnitude is found close to the collective plasmon excitation in the nanoantenna array, rather than at the highest antenna density. Our method establishes a low-cost replacement technique for electron beam lithography. Simple, fast, and straightforward fabrication of optimized SEIRA antenna arrays with cm^2 areas, which can be used in real-world applications such as chemical and biological vibrational sensing, is now possible.

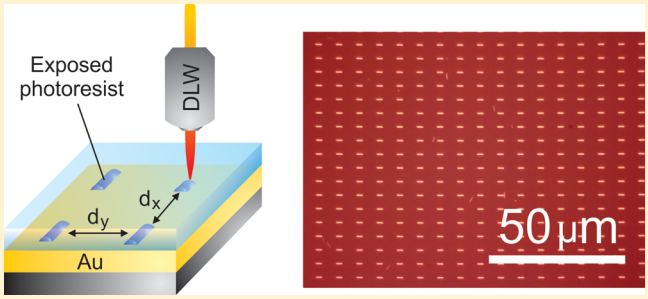

KEYWORDS: *direct laser writing, large-area fabrication, plasmonic nanoantennas, surface-enhanced infrared absorption*

Infrared (IR) spectroscopy is a standard technique in chemistry and life science for the unambiguous identification of materials and molecules based on their specific infrared absorption. The main limitation of infrared spectroscopy, however, is the relative low-absorption cross-section of molecular excitations.[1] Recently, special designs of metal structures, known as plasmonic antennas,[2−4] are employed to overcome this limitation. Such nanoantennas provide huge electromagnetic near fields, which can be used to enhance vibrational signals of molecules located in such hot spots. Following this approach of surface-enhanced infrared absorption (SEIRA), the sensitivity is increased by up to 5 orders of magnitude in comparison to conventional infrared transmittance spectroscopy.[5]

While large-area fabrication methods are required for practical applications of SEIRA, nanoantennas in the above-mentioned studies are typically prepared by electron beam lithography (EBL) and lift-off techniques. This process allows for precise control of the nanostructure geometries but hampers direct and maskless large-area fabrication on reasonable time scales. In principle, state-of-the-art photolithography methods such as used in the semiconductor industry today enable a fast production of decimeter-sized arrays of nanometer-sized and well-defined metal structures. However, mask fabrication for this process is expensive and inflexible, and low-cost access to such facilities is quite limited, particularly on a research level. In contrast to that, randomly distributed metal island films[6,7] can easily be prepared on large scales at low costs but provide relatively low SEIRA enhancement. Nanostructures fabricated by colloidal mask lithography[8,9] or laser interference lithography[10] offer a higher enhancement, but only randomly or particularly arranged nanostructure geometries with low aspect ratios are feasible. Some other methods such as nanostencil lithography[11,12] or direct nanocutting[13] employ a patterned sample as a mask, which needs to be prepared by other techniques, mostly EBL. However, the use of tailored masks allows for a fast nanofabrication on large areas. For example, reconstructable mask lithography proposed by Yang et al.[14] is able to fabricate wafer-scale-sized metamaterial with nanoscale dimensions. Recently, photoinduced fabrication methods have been introduced for SEIRA applications, but the tailored nanostructures fabricated by these methods do not provide a sufficient homogeneity and high SEIRA enhancement at the same time. For example, nanospherical-lens lithography[15] suffers from

Received: March 23, 2015
Published: May 13, 2015

DOI: 10.1021/acsphotonics.5b00141
ACS Photonics 2015, 2, 779−786

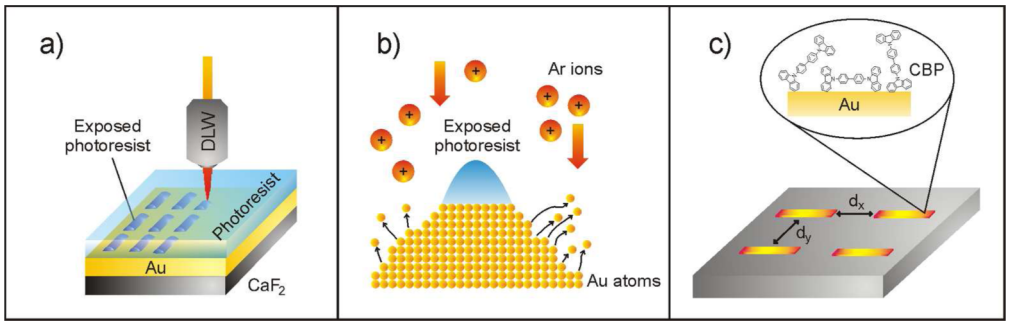

Figure 1. Illustration of the nanoantenna fabrication process using femtosecond direct laser writing (DLW) lithography. (a) The laser beam scans the sample and exposes the photoresist at the gold interface selectively. (b) Argon (Ar) ion beam etching process: after photoresist development the exposed resist is used as an antenna mask during the etching process. Positive Ar ions are accelerated toward the sample and remove gold atoms from the surface. (c) Antennas with different distances (d_x, d_y) are covered by a 5 nm thick 4,4′-bis(*N*-carbazolyl)-1,1′-biphenyl (CBP) layer to investigate the impact of collective excitations on the signal enhancement in surface-enhanced infrared spectroscopy.

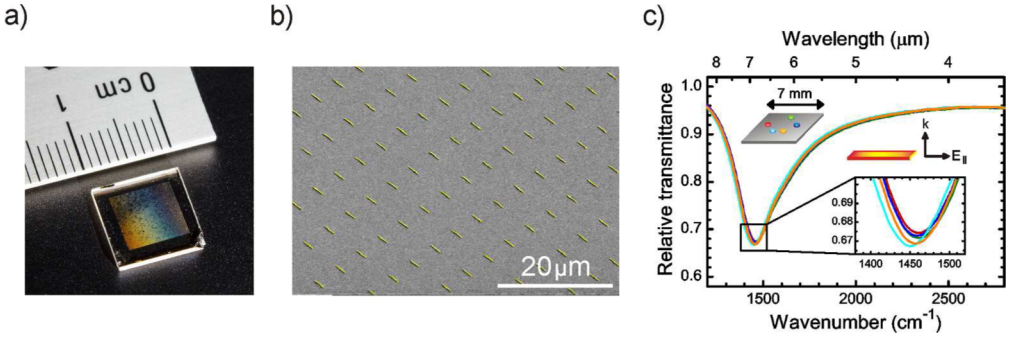

Figure 2. (a) The macrophotograph demonstrates the fabrication of gold nanoantennas on cm^2-sized areas with excellent homogeneity as representatively shown in the tilted view scanning electron micrograph (b) for antennas (2.4 μm length, 140 nm width, and 105 nm height) arranged in arrays with (d_x, d_y) = (5, 5) μm. (c) The homogeneity is also confirmed by relative transmittance spectra ($E_{||}$, parallel polarization) measured at different positions by infrared microscopic spectroscopy (spot size ≈ 100 × 100 μm^2). Typically, the resonance frequency of the plasmonic excitation deviates less than 2%, as seen in the inset.

inhomogeneities, and metal stripe gratings produced by photolithography offer only moderate enhancement.[16]

In contrast to that, direct laser writing (DLW) as a two-photon absorption process allows for a homogeneous and well-controlled fabrication of nanostructures[17,18] over large areas at low costs. In this approach, a tightly focused spot of femtosecond laser light causes local polymerization in a polymer and thus enables the writing of arbitrarily shaped 3D structures, e.g., for perfect absorption,[19] telecommunications,[20] and optical devices for integrated optics.[21−23] However, the preparation of 2D metal nanostructures is easily feasible via selectively scanning the photoresist interface and subsequent argon ion etching as demonstrated in the following. Besides a homogeneous fabrication of nanostructures on large areas, this versatile nanofabrication technique allows for the preparation of arbitrarily arranged nanoantennas. Thus, systematic studies on the impact of various plasmonic coupling effects on the enhancement in surface-enhanced spectroscopic techniques, such as surface-enhanced Raman spectroscopy (SERS),[24] enhanced fluorescence,[25] or SEIRA, are feasible.

Numerous studies during the past decade report on how the optical properties of such specially arranged nanoantennas depend on the interaction with other particles situated in the near[26,27] or far field.[28,29] For SEIRA it was demonstrated that nanoantennas with nanometer-sized gaps increase the enhancement by 1 order of magnitude in comparison to individual antennas.[30] However, also collective plasmonic excitations originating from periodically arranged nanostructures can provide additional SEIRA enhancement[31,32] if the critical grating periodicity Λ_x and Λ_y fulfill the following equation:

$$\frac{n_s}{\lambda_{collective}} \approx \sqrt{\left(\frac{i}{\Lambda_x}\right)^2 + \left(\frac{j}{\Lambda_y}\right)^2} \quad (1)$$

Here, n_s denotes the refractive index of the substrate, i and j are the diffraction grating orders, and $\lambda_{collective}$ is the resonance wavelength of the collective mode. Nanoantennas with resonances tuned to this Rayleigh anomaly[33] strongly enhance the collective plasmonic response, which results in an efficient funneling of incident light into stronger near field excitations. The effect was first exploited for SEIRA by Adato et al.,[32] employing nanoantenna arrays with identical periodicities perpendicular (Λ_y) and parallel (Λ_x) to the long antenna axis, whereas in the present study both periodicities are varied individually.

In the present paper, we demonstrate how direct laser writing lithography combined with argon ion etching can be used as a reliable method to prepare homogeneous large-area arrays of plasmonic nanoantennas for vibrational sensing in the mid-infrared range. Enabled by the versatility of DLW with respect to the arrangement of nanostructures, we fabricate nanoantenna arrays with different longitudinal and transversal spacings. After the evaporation of the molecular probe named 4,4′-bis(*N*-carbazolyl)-1,1′-biphenyl (CBP), their SEIRA activity is measured and then evaluated regarding the optimum configuration for SEIRA.

DOI: 10.1021/acsphotonics.5b00141
ACS Photonics 2015, 2, 779−786

RESULTS AND DISCUSSION

An illustrated drawing of the two-photon direct laser writing process is shown in Figure 1a. The femtosecond laser light selectively exposes the photoresist, and a photoresist mask is generated via scanning the interface between the photoresist and the gold-coated calcium difluoride (CaF_2) substrate. After the development process, the exposed photoresist remains on the surface and is used as a mask for argon ion beam etching (Figure 1b), enabling the fabrication of gold nanoantennas with well-defined geometrical parameters. In order to prepare large-area samples required for practical applications, the maximum scanning area (200 × 200 μm) is subsequently extended by using a positioner stage that moves up to several centimeters.

Following this approach, we fabricate homogeneous nanoantenna arrays on large areas as shown exemplarily in the photograph and a scanning electron microscope (SEM) image (Figure 2a and b, respectively). The large-area sample is fabricated by stitching 2601 fields next to each other. Each field has a size of 150 × 150 μm^2; hence the antenna array covers 7.6 × 7.6 mm^2. In order to prevent stitching errors, the whole area is designed in such a way that only small movements of the mechanical stage are necessary and additionally the stage is always moved from one direction to each field. Typical DLW illumination times of such cm^2-sized samples are 1 order of magnitude smaller than standard EBL exposure times. Their remarkable homogeneity is also confirmed by their infrared optical properties measured at different positions with average distances of about 2 mm (Figure 2c and Supporting Information S1). As seen in the inset, the resonance frequencies (transmittance minimum) deviate less than 2% over the sample, confirming the excellent homogeneity of our nanoantennas on large scales.

Precise tunability of plasmonic properties is desirable for any sensing application but requires full control over their geometry.[12] Direct laser writing combined with argon ion etching offers such versatile control during the fabrication process. On one hand, specific illumination times and laser powers in the DLW process result in different antenna lengths (L) and widths (W), respectively. Keeping the argon ion beam etching time at 210 s, for example, but changing the DLW illumination power from 9 to 5 mW (in steps of 1 mW) enables us to prepare nanoantennas with widths changing from 335 to 150 nm. Such nanoantennas with design lengths between 1.7 and 2.8 μm feature tunable plasmon resonances in the mid-IR spectral range, as shown in Figure 3a. For more details on the nanofabrication process see the methods.

On the other hand, antenna geometries can be controlled by the argon ion etching process. The widths of antennas can be further narrowed by higher argon etching times, 255 s instead of 210 s, but the same laser powers during direct laser writing. Figure 3b shows typical SEM images (selected antenna arrays) and typical relative transmittance spectra of such antennas measured in parallel polarization. Their widths vary from 105 to 290 nm, demonstrating the capability of our approach to prepare antennas with feature sizes below the diffraction limit of the femtosecond laser light. Please note that longer argon etching times slightly decrease the antenna lengths. However, this is only a small absolute change (50 nm) compared to the design length (micrometer range) and thus does not influence the resonance properties significantly.

In order to demonstrate the SEIRA activity of our nanoantennas, we evaporated a homogeneous layer of CBP

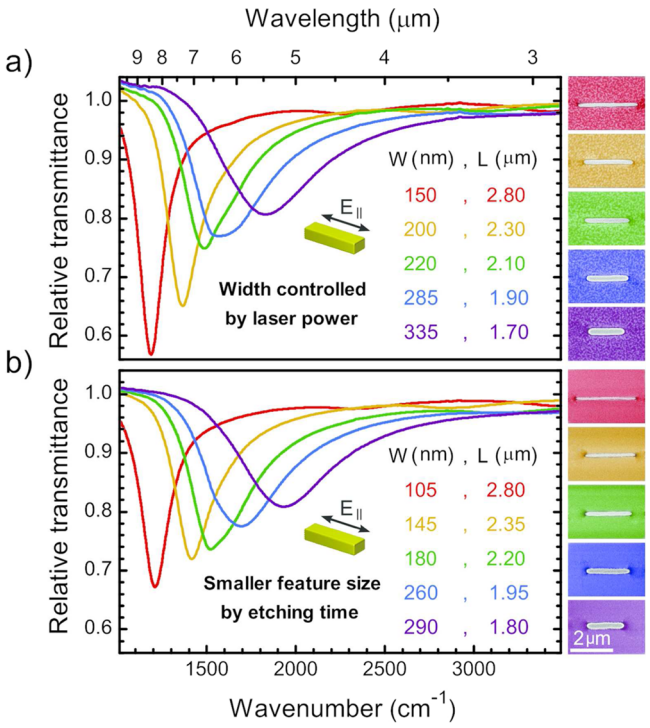

Figure 3. SEM images (right) and relative transmittance spectra ($E_{||}$, parallel polarization) of nanoantennas with widths below the diffraction limit of radiation used in the direct laser writing lithography process are shown. The width (W) of each antenna can be defined independently of the length (L) by changing the laser power (a) and further narrowed by increasing the etching time (210 to 255 s) (b). Lengths and widths of the antennas are varied from 1.7 to 2.8 μm and 105 to 335 nm, respectively. The laser powers in (a) and (b) are varied from 9 to 5 mW (in steps of 1 mW), resulting in narrower antennas for lower illumination powers. The height of the narrowest antenna is 75 nm, for all other antennas it is approximately 105 nm, and the distances between antennas are (d_x, d_y) = (5, 5) μm.

(thickness 5 nm) on antenna arrays with various lengths and spacings (see Figure 1c). For more details on the CBP evaporation process, see Figure S2 in the Supporting Information and ref 30. Since the optical properties of nanoantenna arrays strongly depend on the plasmonic coupling caused by their periodical arrangement, we expect a similar behavior for their SEIRA enhancement.[31,34] To independently investigate the effects of longitudinal (parallel to long antenna axis) and transversal (perpendicular to long antenna axis) plasmonic coupling on SEIRA, the spacing along the long antenna axis (d_x) and the short antenna axis (d_y) is varied individually from 0.5 to 10 μm (Figure 1c). Additionally, the fabrication of different antenna lengths for each configuration (d_x, d_y) ensures a good match of the plasmonic resonances and selected CBP vibrations (combined CH deformation and CN stretching mode at 1504 cm^{-1} as well as CH deformation mode at 1230 and 1450 cm^{-1}), which is necessary for an optimum SEIRA enhancement. For this preparation task, DLW combined with argon ion etching is ideally suited, since it provides full flexibility regarding antenna arrangement and geometry on reasonable time scales.

Representative SEM images of four selected nanoantenna arrays with similar lengths (L = 2.6 μm) but different spacings (d_x, d_y) and their corresponding transmission spectra are shown in Figure 4.

DOI: 10.1021/acsphotonics.5b00141
ACS Photonics 2015, 2, 779−786

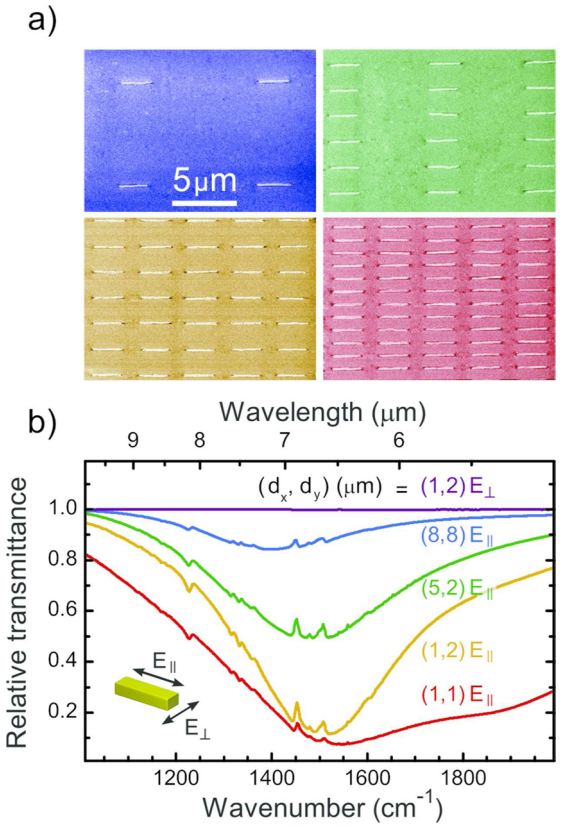

Figure 4. (a) Representative SEM images of nanoantennas with selected antenna distances prepared by direct laser writing lithography for our SEIRA studies. (b) Relative transmittance spectra of the corresponding antennas (2.6 μm length, 140 nm width, antenna spacings in μm are indicated by colored numbers in the plot) covered with a 5 nm thick layer of CBP acting as a probe for the SEIRA enhancement. Depending on the antenna distances, different enhancements of the CBP vibrational bands are found for parallel polarization ($E_{\parallel}$), whereas no enhanced signals are found for perpendicular polarization ($E_{\perp}$, purple curve).

IR measurements in perpendicular polarization (purple curve) do not provide infrared plasmonic resonances, and thus no enhanced CBP vibrations are detected. In contrast to that, broadband plasmonic resonances are excited with parallel polarized light. Here, the CBP absorption bands are enhanced by the plasmonic near fields. In the spectra, they appear as sharp features on the antenna resonance curve with Fano-type line-shapes originating from the coupling between the plasmonic and the vibrational excitation.[5,35] As expected, arrays with higher antenna densities mostly show higher signal intensities. However, this correlation does not hold for distances smaller than (d_x, d_y) = (1, 2) μm. For example, although configurations (1, 1) and (1, 2) have the same extinction, the enhanced vibrational signals of configuration (1, 2) are significantly stronger despite the lower antenna density. Consequently, plasmonic interactions between nanoantennas, which considerably change the IR optical properties, must play a significant role in the SEIRA enhancement.

In order to investigate this effect, we extract the enhanced vibrational signals from the baseline-corrected transmittance and normalize them to nonenhanced CBP vibrations (see Figure S2 in the Supporting Information) as well as to the antenna density given by (d_x, d_y). In more detail, we approximated the baseline of the antenna resonance using an adoption of the computational approach of asymmetric least-squares smoothing[36] while excluding the spectral regions of the selected vibrational bands. As an example we show the measured spectra of (d_x, d_y) = (1, 2) μm for different antenna lengths in Figure 5a (top panel) and the corresponding

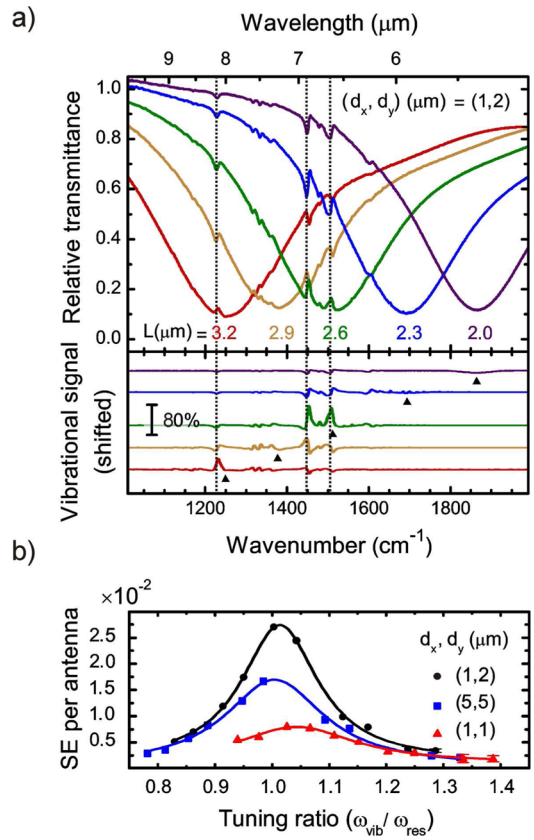

Figure 5. Surface-enhanced infrared spectroscopy of CBP-covered nanoantennas in dependence on the tuning between the plasmonic and molecular excitation. (a) Upper panel: Relative transmittance spectra (parallel polarization) of representative antenna arrays with same distances (d_x, d_y) = (1, 2) μm and antenna widths (140 nm) but different lengths L as indicated. Lower panel: Corresponding baseline-corrected IR spectra with resonance positions indicated by black triangles. Due to the differences in resonance matching of the antennas, different enhanced signals and line-shapes are observed. Dotted lines indicate the spectral positions of the CBP vibrations of interest at 1230, 1450, and 1504 cm^{-1}. (b) Signal enhancements (SE) per antenna (enhanced vibrational signal normalized to a reference measurement of a 5 nm CBP layer on unstructured CaF_2) of the strongest CBP vibrational bands (1450 and 1504 cm^{-1}) versus tuning ratio (ratio of vibration frequency to resonance frequency) with (d_x, d_y) as given in the legend. The solid lines are Lorentzian fits for better visualization.

baseline-corrected signals (bottom panel) obtained by the ratio between the measured transmission spectrum and the fitted baseline. The vibrational signals of the baseline-corrected spectra exhibit a typical asymmetric Fano shape.[5,35] As seen in the upper panel, the signal enhancement strongly depends on the match between vibrational frequency (ω_{vib}) and the plasmonic resonance frequency (ω_{res}). This becomes even more obvious in Figure 5b, where the signal enhancement per antenna of the CBP vibration at 1450 and 1504 cm^{-1} in dependence on the tuning ratio ($\omega_{vib}/\omega_{res}$) is plotted for selected configurations (d_x, d_y). As expected, the signal

DOI: 10.1021/acsphotonics.5b00141
ACS Photonics 2015, 2, 779−786

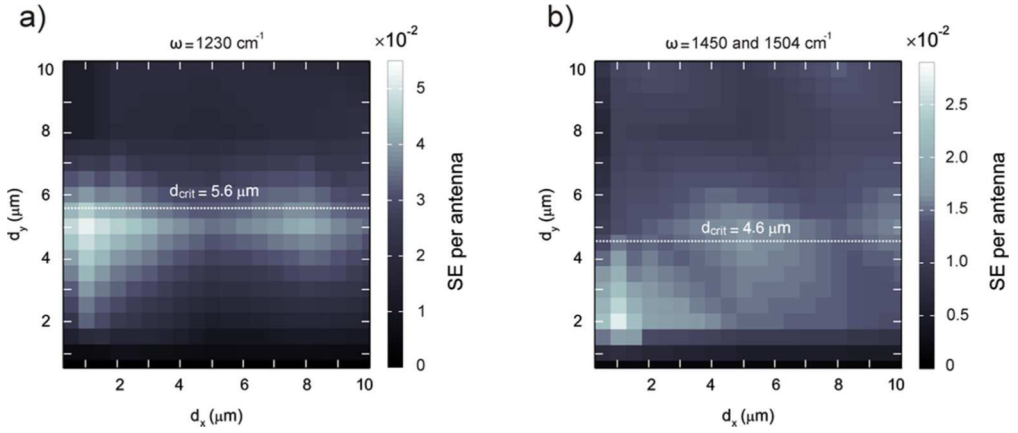

Figure 6. Signal enhancement (SE) per antenna of the vibrations at (a) 1230 cm^{-1} and (b) 1450 and 1504 cm^{-1} over the longitudinal d_x and transversal d_y spacing. Due to the close spectral vicinity of the vibrations at 1450 and 1504 cm^{-1}, both modes are grouped together (see text). Notably high values are found in (a) for d_y = 5 μm and in (b) for d_y = 2 μm, with the highest signal enhancement at (d_x, d_y) = (1, 5) (μm) and (1, 2) (μm), respectively, indicating a significant influence of the collective plasmonic excitation in antenna arrays on the signal enhancement. The total enhancement is the signal enhancement per antenna multiplied with the total number of antennas that participate in the collective resonance, which ranges typically on the order of 100 to 4000. The dashed lines indicate the calculated critical grating distances d_{crit} ($d_{crit,y} = \Lambda_y - W$ and $d_{crit,x} = \Lambda_x - L$). The area between the measurement points is linearly interpolated.

enhancement per antenna peaks around a tuning ratio of 1, corresponding to a perfect match between vibrational and resonance frequency.

Finally, by taking the maximum values determined in Figure 5b, we obtain the signal enhancement per antenna over the longitudinal and transversal spacings between antennas (see Figure 6). Notably high values are found close to d_y = 5 μm for the vibration at ω = 1230 cm^{-1} (Figure 6a) and d_y = 2 μm for the vibrations at ω = 1450 cm^{-1} and ω = 1504 cm^{-1}, respectively (Figure 6b). The appearance of the enhancement maxima can be explained by the excitation of collective resonances in metal arrays, namely, the Rayleigh anomalies.[37,38] As discussed in the introduction, stronger near fields and thus stronger SEIRA enhancements[39,40] are found for nanoantennas arranged with the critical grating periodicity. In a first approximation, we consider only the interaction between next neighbors and neglect the contributions from longitudinal coupling, since a dipole antenna radiates preferentially perpendicular to its axis of polarization.[34,41] According to eq 1, we deduce a critical grating distance $d_{crit} \approx 5.6$ μm (difference of critical grating periodicity Λ_y and antenna width W) for the maximum signal enhancement per antenna of the CH deformation vibration at 1230 cm^{-1}, which is in good agreement with our experimental data (see Figure 6a). Slight deviations may originate from an angle dependency of the collective plasmonic excitation.[41] For the vibrations located at 1450 and 1504 cm^{-1}, which can be pooled due to their spectral vicinity, one calculates $d_{crit} \approx 4.6$ μm as the critical grating distance. Obviously, this estimated critical spacing deviates from our experimentally determined maximum signal enhancement per antenna (Figure 6b). As shown by Adato et al.,[41] spacings slightly larger than the critical grating distance result in a strong damping of the collective plasmonic resonances and a loss of the additional near field enhancement. Thus, only a relatively small spectral window provides additional enhancement, which was not precisely matched to the antenna resonance and the vibrational bands at 1450 and 1504 cm^{-1} in our experiments. However, the maximum signal enhancements per antenna of different vibrations scale with the critical grating distance, as expected from eq 1 and qualitatively seen in Figure 6. Furthermore, the maximum value differs due to the stronger near fields found for longer antenna lengths.[42]

For both plots, a remarkably sharp drop is observed for transversal spacings d_y smaller than 2 μm, while the effect is much less prominent for longitudinal spacings d_x. This result is in agreement with previous studies,[32,34] where a strong broadening of the plasmonic resonances and a decrease of the near field intensity were found for small spacings d_y induced by transversal coupling. In contrast to that, longitudinal coupling over micrometer-sized d_x only marginally affects the antenna resonance and near field enhancement.[34] However, a further decrease of d_x down to several tens of nanometers, which is not the subject of the present study, results in higher SEIRA enhancements due to near field coupling, as shown for example in ref 30. For larger separations of d_y, the benefit of a plasmonic interaction vanishes and the signal enhancement per antenna decreases. Nevertheless, also the limit of a single nanoantenna is of potential interest, since here the absolute amount of detectable molecules is lowest.

Please note that the signal enhancement (not normalized to one antenna) peaks at slightly smaller spacings (see Figure S3 in the Supporting Information), but the above-mentioned behavior still holds. For example, smaller distances do not necessarily provide higher signals, even though more antenna hot spots are available for enhancement. This is in contrast to other studies with periodically arranged ITO nanoparticles acting as SEIRA substrates.[31] There, the signal enhancement scales with the antenna density, since collective plasmonic excitations are negligible due to the high absorption but low scattering of the particles.

Finally, we representatively estimated a SEIRA enhancement factor by taking into account the molecules located in the confined electromagnetic near fields of the antennas. Only molecules situated in these active areas contribute to the enhanced vibrational signal. Therefore, we multiply the maximum signal enhancement per antenna (SE ≈ 0.04), which is found for the (d_x, d_y) = (1, 5) μm configuration and ω = 1230 cm^{-1}, by the used spot size (A_0 = 100 × 100 μm^2). Assuming an active area 2 times the antenna end faces according to ref 43 and a homogeneous coverage, we find an

DOI: 10.1021/acsphotonics.5b00141
ACS Photonics 2015, 2, 779−786

enhancement factor of 14 000, in agreement with other studies.[10,32,44]

CONCLUSION

In conclusion, we combine femtosecond direct laser writing and argon ion beam etching to fabricate homogeneous large-area nanoantenna arrays, providing plasmon resonances in the mid-infrared spectral range. Such nanoantennas are ideally suited as substrates for surface-enhanced infrared absorption, as demonstrated by enhancing vibrational signals of CBP molecules evaporated on antenna arrays with different spacings between the elements. The signal enhancement is strongly influenced by plasmonic coupling that originates from the periodical arrangement of antennas and is maximum close to the Rayleigh anomaly. For this optimum configuration, we find a maximum SEIRA enhancement factor of about 4 orders of magnitude, which is comparable to the SEIRA activity of substrates prepared with other nanofabrication methods such as interference lithography, colloidal hole mask lithography, or electron-beam lithography.

METHODS

Sample Fabrication. CaF_2 substrates (refractive index n_s = 1.42) were cleaned with acetone and 2-propanol for 10 min in an ultrasonic bath. After drying with nitrogen, we evaporated 5 nm of Cr as an adhesion layer and a 100 nm thick layer of gold (Pfeiffer vacuum model PLS-500, 10^{-7} mbar) as a plasmonic material onto the substrate. A drop of photoresist (Nanoscribe IP-Dip), needed for the dip-in direct laser writing process,[45] was then cast on top of the gold surface.

For direct laser writing, we used a Photonic Professional GT machine (Nanoscribe GmbH, Germany) with a femtosecond laser beam (λ = 780 nm), which was focused by an objective lens (63-fold magnification, NA = 1.4) into the photoresist. The tunable laser power at the entrance of the objective was between 5 and 9 mW, resulting in different thicknesses (175 to 105 nm) and line widths (full widths at half-maximum between 305 and 245 nm) of the exposed photoresist mask after development. The typical writing speed was 12000 μm/s, enabling the illumination of a 7.6 × 7.6 mm^2 sized sample within 90 min using stitching techniques as described in the text.

After the illumination process, we kept the samples in the developer (Microresist mr-dev 600) for 15 min and in 2-propanol for 2 min to remove the nonilluminated areas. The patterned areas were used as a mask and transferred into the gold layer via an argon ion beam etching process (Technics Plasma model R.I.B.-Etch 160, beam current range from 90 to 100 mA, typical etching times between 200 and 300 s). The etching rates are 0.5 nm/s for gold, 0.24 nm/s for CaF_2, and 0.54 nm/s for the polymer, measured by atomic force microscopy. Thus, the etching ratios of exposed photoresist to gold and to CaF_2 are approximately 1:1 and 2:1, respectively. The remaining polymer was removed using oxygen plasma (Diener Electronic Plasma-Surface-Technology, 90 min, 1.4 mbar, 160 W). As a result, we obtained antenna arrays with typical antenna lengths and widths in the range 1.7 to 2.8 μm and 105 to 350 nm, respectively. Also the spacing along the long (d_x) and short (d_y) antenna axis was varied individually. For both directions we chose six different distances (0.5, 1, 2, 5, 8, and 10 μm), resulting in 36 different configurations for (d_x, d_y) with five lengths per configuration. The antenna heights were approximately 105 nm. For the initial design, the geometrical parameters were estimated by Fourier modal method simulations.[46]

CBP Evaporation. 4,4′-Bis(*N*-carbazolyl)-1,1′-biphenyl (Sigma-Aldrich, 99.9%) was evaporated under ultra-high-vacuum conditions. For more details, see ref 30.

IR Transmittance Measurements. IR optical properties were measured using a Bruker Hyperion 2000 IR microscope (Schwarzschild-objective with 15-fold magnification, NA = 0.4) coupled to a Bruker Vertex 80 spectrometer with an optical path purged with nitrogen. To obtain the relative transmittance spectra, the transmittance at the position of the CBP-covered nanoantenna is normalized to an unstructured but CBP-covered area close to the nanostructures. A typical spot size is 100 × 100 μm^2 for the SEIRA measurements, allowing the illumination of about 500 antennas for (d_x, d_y) = (1, 5) μm. All spectra were acquired with an IR polarizer (working range 2 to 10 μm) and a liquid-nitrogen-cooled mercury cadmium telluride detector with at least 25 scans and a resolution of 2 cm^{-1}. For the acquisition of the nonenhanced CBP spectrum, we used an area without nanostructures on the sample and a bare CaF_2 wafer as reference.

Photograph and Scanning Electron Micrographs. The photograph was taken with a Canon EOS 60D camera with a Canon EF100 mm f/2.8 Macro USM (f/8, 1/4 s, ISO 100). The sample was illuminated with a white LED light source. The scanning electron micrographs were acquired with an S-4800 scanning electron microscope (Hitachi Company). Charged areas in the SEM image were removed for a better visualization.

ASSOCIATED CONTENT

Supporting Information

Relative transmittance spectrum of a large-area sample measured with a low-cost FTIR spectrometer (Bruker alpha), IR optical properties of CBP, and laterally resolved signal enhancement. The Supporting Information is available free of charge on the ACS Publications website at DOI: 10.1021/acsphotonics.5b00141.

AUTHOR INFORMATION

Corresponding Author

*E-mail: h.giessen@pi4.uni-stuttgart.de.

Author Contributions

The manuscript was written through contributions of all authors. All authors have given approval to the final version of the manuscript.

Author Contributions

‡S. Bagheri and K. Weber contributed equally to this work.

Notes

The authors declare no competing financial interest.

ACKNOWLEDGMENTS

The authors gratefully acknowledge financial support by ERC Advanced Grant COMPLEXPLAS as well as DFG, BMBF, GIF, Zeiss Foundation, and MWK Baden-Württemberg and the Baden-Württemberg Stiftung (PROTEINSENS, Spitzenforschung II). The CBP deposition was done under the guidance of Tobias Glaser at the clustertool of the BMBF MESOMERIE Project (FKZ 13N10724) hosted by the InnovationLab GmbH, Heidelberg, Germany. The authors also thank Dominik Floess for sample photography.

DOI: 10.1021/acsphotonics.5b00141
ACS Photonics 2015, 2, 779−786

REFERENCES

(1) Smith, B. C. *Fundamentals of Fourier Transform Infrared Spectroscopy*, second ed.; CRC Press, Boca Raton, 2011.

(2) Pryce, I. M.; Kelaita, Y. A.; Aydin, K.; Atwater, H. A. Compliant metamaterials for resonantly enhanced infrared absorption spectroscopy and refractive index sensing. *ACS Nano* **2011**, *5*, 8167−8174.

(3) Cubukcu, E.; Zhang, S.; Park, Y.-S.; Bartal, G.; Zhang, X. Split ring resonator sensors for infrared detection of single molecular monolayers. *Appl. Phys. Lett.* **2009**, *95*, 043113.

(4) Aouani, H.; Rahmani, M.; Šípová, H.; Torres, V.; Hegnerová, K.; Beruete, M.; Homola, J.; Hong, M.; Navarro-Cía, M.; Maier, S. A. Plasmonic nanoantennas for multispectral surface-enhanced spectroscopies. *J. Phys. Chem. C* **2013**, *117*, 18620−18626.

(5) Neubrech, F.; Pucci, A.; Cornelius, T. W.; Karim, S.; García-Etxarri, A.; Aizpurua, J. Resonant plasmonic and vibrational coupling in a tailored nanoantenna for infrared detection. *Phys. Rev. Lett.* **2008**, *101*, 157403.

(6) Hoang, C. V.; Oyama, M.; Saito, O.; Aono, M.; Nagao, T. Monitoring the presence of ionic mercury in environmental water by plasmon-enhanced infrared spectroscopy. *Sci. Rep.* **2013**, *3*, 1175.

(7) Perry, D. A.; Borchers, R. L.; Golden, J. W.; Owen, A. R.; Price, A. S.; Henry, W. A.; Watanabe, F.; Biris, A. S. Surface-enhanced infrared absorption on elongated nickel nanostructures. *J. Phys. Chem. Lett.* **2013**, *4*, 3945−3949.

(8) Cataldo, S.; Zhao, J.; Neubrech, F.; Frank, B.; Zhang, C.; Braun, P. V.; Giessen, H. Hole-mask colloidal nanolithography for large-area low-cost metamaterials and antenna-assisted surface-enhanced infrared absorption substrates. *ACS Nano* **2012**, *6*, 979−985.

(9) Hoffmann, J. M.; Yin, X.; Richter, J.; Hartung, A.; Maß, T. W. W.; Taubner, T. Low-cost infrared resonant structures for surface-enhanced infrared absorption spectroscopy in the fingerprint region from 3 to 13 μm. *J. Phys. Chem. C* **2013**, *117*, 11311−11316.

(10) Bagheri, S.; Giessen, H.; Neubrech, F. Large-area antenna-assisted SEIRA substrates by laser interference lithography. *Adv. Opt. Mater.* **2014**, *2*, 1050−1056.

(11) Aksu, S.; Yanik, A. A.; Adato, R.; Artar, A.; Huang, M.; Altug, H. High-throughput nanofabrication of infrared plasmonic nanoantenna arrays for vibrational nanospectroscopy. *Nano Lett.* **2010**, *10*, 2511−2518.

(12) Aksu, S.; Cetin, A. E.; Adato, R.; Altug, H. Plasmonically enhanced vibrational biospectroscopy using low-cost infrared antenna arrays by nanostencil lithography. *Adv. Opt. Mater.* **2013**, *1*, 798−803.

(13) Auzelyte, V.; Gallinet, B.; Flauraud, V.; Santschi, C.; Dutta-Gupta, S.; Martin, O. J. F.; Brugger, J. Large-area Gold/Parylene plasmonic nanostructures fabricated by direct nanocutting. *Adv. Opt. Mater.* **2013**, *1*, 50−54.

(14) Yang, A.; Huntington, M. D.; Cardinal, M. F.; Masango, S. S.; Van Duyne, R. P.; Odom, T. W. Hetero-oligomer nanoparticle arrays for plasmon-enhanced hydrogen sensing. *ACS Nano* **2014**, *8*, 7639−7647.

(15) Chang, Y.-C.; Lu, S.-C.; Chung, H.-C.; Wang, S.-M.; Tsai, T.-D.; Guo, T.-F. High-throughput nanofabrication of infrared and chiral metamaterials using nanospherical-lens lithography. *Sci. Rep.* **2013**, *3*, 3339.

(16) Wang, T.; Nguyen, V. H.; Buchenauer, A.; Schnakenberg, U.; Taubner, T. Surface enhanced infrared spectroscopy with gold strip gratings. *Opt. Express* **2013**, *21*, 9005−9010.

(17) Kenanakis, G.; Xomalis, A.; Selimis, A.; Vamvakaki, M.; Farsari, M.; Kafesaki, M.; Soukoulis, C. M.; Economou, E. N. Three-dimensional infrared metamaterial with asymmetric transmission. *ACS Photonics* **2015**, *2*, 287−294.

(18) Cui, Y.; Phang, I. Y.; Hegde, R. S.; Lee, Y. H.; Ling, X. Y. Plasmonic silver nanowire structures for two-dimensional multiple-digit molecular data storage application. *ACS Photonics* **2014**, *1*, 631−637.

(19) Xiong, X.; Jiang, S.-C.; Hu, Y.-H.; Peng, R.-W.; Wang, M. Structured metal film as a perfect absorber. *Adv. Mater.* **2013**, *25*, 3994−4000.

(20) Deubel, M.; von Freymann, G.; Wegener, M.; Pereira, S.; Busch, K.; Soukoulis, C. M. Direct laser writing of three-dimensional photonic-crystal templates for telecommunications. *Nat. Mater.* **2004**, *3*, 444−447.

(21) Thiel, M.; Rill, M. S.; von Freymann, G.; Wegener, M. Three-dimensional bi-chiral photonic crystals. *Adv. Mater.* **2009**, *21*, 4680−4682.

(22) Schumann, M.; Bückmann, T.; Gruhler, N.; Wegener, M.; Pernice, W. Hybrid 2D−3D optical devices for integrated optics by direct laser writing. *Light Sci. Appl.* **2014**, *3*, 175.

(23) Radke, A.; Gissibl, T.; Klotzbücher, T.; Braun, P. V.; Giessen, H. Three-dimensional bichiral plasmonic crystals fabricated by direct laser writing and electroless silver plating. *Adv. Mater.* **2011**, *23*, 3018−3021.

(24) Theiss, J.; Pavaskar, P.; Echternach, P. M.; Muller, R. E.; Cronin, S. B. Plasmonic nanoparticle arrays with nanometer separation for high-performance SERS substrates. *Nano Lett.* **2010**, *10*, 2749−2754.

(25) Cui, X. Q.; Tawa, K.; Hori, H.; Nishii. Tailored plasmonic gratings for enhanced fluorescence detection and microscopic imaging. *Adv. Funct. Mater.* **2010**, *20*, 546−553.

(26) Su, K. H.; Wei, Q. H.; Zhang, X.; Mock, J. J.; Smith, D. R.; Schultz, S. Interparticle coupling effects on plasmon resonances of nanogold particles. *Nano Lett.* **2003**, *3*, 1087−1090.

(27) Li, Z.; Butun, S.; Aydin, K. Touching gold nanoparticle chain based plasmonic antenna arrays and optical metamaterials. *ACS Photonics* **2014**, *1*, 228−234.

(28) Hicks, E. M.; Zou, S.; Schatz, G. C.; Spears, K. J.; Van Duyne, R. P.; Gunnarsson, L.; Rindzeviciu, T.; Kasemo, B.; Käll, M. Controlling plasmon line shapes through diffractive coupling in linear arrays of cylindrical nanoparticles fabricated by electron beam lithography. *Nano Lett.* **2005**, *5*, 1065−1070.

(29) Pirzadeh, Z.; Pakizeh, T.; Miljkovic, V.; Langhammer, C.; Dmitriev, A. Plasmon−interband coupling in nickel nanoantennas. *ACS Photonics* **2014**, *1*, 158−162.

(30) Huck, C.; Neubrech, F.; Vogt, J.; Toma, A.; Gerbert, D.; Katzmann, J.; Hartling, T.; Pucci, A. Surface-enhanced infrared spectroscopy using nanometer-sized gaps. *ACS Nano* **2014**, *8*, 4908−4914.

(31) Abb, M.; Wang, Y.; Papasimakis, N.; de Groot, C. H.; Muskens, O. L. Surface-enhanced infrared spectroscopy using metal oxide plasmonic antenna arrays. *Nano Lett.* **2014**, *14*, 346−352.

(32) Adato, R.; Yanik, A. A.; Amsden, J. J.; Kaplan, D. L.; Omenetto, F. G.; Hong, M. K.; Erramilli, S.; Altug, H. Ultra-sensitive vibrational spectroscopy of protein monolayers with plasmonic nanoantenna arrays. *Proc. Natl. Acad. Sci. U.S.A.* **2009**, *106*, 19227−19232.

(33) Kichin, G.; Weiss, T.; Gao, H.; Henzie, J.; Odom, T. W.; Tikhodeev, S. G.; Giessen, H. Metal-dielectric photonic crystal superlattice: 1D and 2D models and empty lattice approximation. *Phys. B (Amsterdam, Neth.)* **2012**, *407*, 4037−4042.

(34) Weber, D.; Albella, P.; Alonso-González, P.; Neubrech, F.; Gui, H.; Nagao, T.; Hillenbrand, R.; Aizpurua, J.; Pucci, A. Longitudinal and transverse coupling in infrared gold nanoantenna arrays: long range versus short range interaction regimes. *Opt. Express* **2011**, *19*, 15047−15061.

(35) Giannini, V.; Francescato, Y.; Amrania, H.; Phillips, C. C.; Maier, S. A. Fano resonances in nanoscale plasmonic systems: a parameter-free modeling approach. *Nano Lett.* **2011**, *11*, 2835−2840.

(36) Eilers, P. H. C. A perfect smoother. *Anal. Chem.* **2003**, *75*, 3631−3636.

(37) Giannini, V.; Vecchi, G.; Gómez Rivas. Lighting up multipolar surface plasmon polaritons by collective resonances in arrays of nanoantennas. *J. Phys. Rev. Lett.* **2010**, *105*, 266801.

(38) Lovera, P.; Jones, D.; Corbett, B.; O'Riordan, A. Polarization tunable transmission through plasmonic arrays of elliptical nanopores. *Opt. Express* **2012**, *20*, 25325−25332.

(39) Alonso-González, P.; Albella, P.; Schnell, M.; Chen, J.; Huth, F.; Garca-Etxarri, A.; Casanova, F.; Golmar, F.; Arzubiaga, L.; Hueso, L. E.; Aizpurua, J.; Hillenbrand, R. Resolving the electromagnetic mechanism of surface-enhanced light scattering at single hot spots. *Nat. Commun.* **2012**, *3*, 684.

DOI: 10.1021/acsphotonics.5b00141
ACS Photonics 2015, 2, 779−786

(40) Dregely, D.; Neubrech, F.; Duan, H.; Vogelgesang, R.; Giessen, H. Vibrational near-field mapping of planar and buried 3D plasmonic nanostructures. *Nat. Commun.* **2013**, *4*, 2237.
(41) Adato, R.; Yanik, A. A.; Wu, C. H.; Shvets, G.; Altug, H. Radiative engineering of plasmon lifetimes in embedded nanoantenna arrays. *Opt. Express* **2010**, *18*, 4526−4537.
(42) Alonso-Gonzalez, P.; Albella, P.; Neubrech, F.; Huck, C.; Chen, J.; Golmar, F.; Casanova, F.; Hueso, L. E.; Pucci, A.; Aizpurua, J.; Hillenbrand, R. Experimental verification of the spectral shift between near- and far-field peak intensities of plasmonic infrared nanoantennas. *Phys. Rev. Lett.* **2013**, *110*, 203902.
(43) D'Andrea, C.; Bochterle, J.; Toma, A.; Huck, C.; Neubrech, F.; Messina, E.; Fazio, B.; Maragò, O. M.; Fabrizio, E. D.; de la Chapelle, M. L.; Gucciardi, P. G.; Pucci, A. Optical nanoantennas for multiband surface-enhanced infrared and Raman spectroscopy. *ACS Nano* **2013**, *7*, 3522−3531.
(44) Neubrech, F.; Kolb, T.; Lovrincic, R.; Fahsold, G.; Pucci, A.; Aizpurua, J.; Cornelius, T. W.; Toimil-Molares, M. E.; Neumann, R.; Karim, S. Resonances of individual metal nanowires in the infrared. *Appl. Phys. Lett.* **2006**, *89*, 253104.
(45) Bückmann, T.; Stenger, N.; Kadic, M.; Kaschke, J.; Frölich, A.; Kennerknecht, T.; Eberl, C.; Thiel, M.; Wegener, M. Tailored 3D mechanical metamaterials made by dip-in direct-laser-writing optical lithography. *Adv. Mater.* **2012**, *24*, 2710−2714.
(46) Weiss, T.; Granet, G.; Gippius, N. A.; Tikhodeev, S.; Giessen, H. Matched coordinates and adaptive spatial resolution in the Fourier modal method. *Opt. Express* **2009**, *17*, 8051−8061.

DOI: 10.1021/acsphotonics.5b00141
ACS Photonics 2015, 2, 779−786